2013 IEEE International Conference on Robotics and Automation (ICRA)
Karlsruhe, Germany, May 6-10, 2013

Compliant Humanoid COMAN: Optimal Joint Stiffness Tuning for Modal Frequency Control

Nikos G. Tsagarakis, Stephen Morfey, Gustavo Medrano Cerda, Zhibin Li and Darwin G. Caldwell
Istituto Italiano di Tecnologia (IIT)

***Abstract*— The incorporation of passive compliance in robotic systems could improve their performance during interactions and impacts, for energy storage and efficiency, and for general safety for both the robots and humans. This paper presents the recently developed COMpliant huMANoid COMAN. COMAN is actuated by passive compliance actuators based on the series elastic actuation principle (SEA). The design and implementation of the overall body of the robot is discussed including the realization of the different body segments and the tuning of the joint distributed passive elasticity. This joint stiffness tuning is a critical parameter in the performance of compliant systems. A novel systematic method to optimally tune the joint elasticity of multi-dof SEA robots based on resonance analysis and energy storage maximization criteria forms one of the key contributions of this work. The paper will show this method being applied to the selection of the passive elasticity of COMAN legs. The first completed robot prototype is presented accompanied by experimental walking trials to demonstrate its operation.**

I. Introduction

During the past two decades there has been considerable progress in the mechatronic development of humanoids and bipeds, with robots based on designs ranging from those with entirely passive dynamics to fully powered systems having been explored. The first modern humanoid, WABOT-1 formed the template for most subsequent designs. Hence, ASIMO, which is one of the best performing powered humanoids, was developed from E0 (1986), E1-E2-E3 (1987-1991), E4-E5-E6 (1991-1993), P1-P2-P3 (1993-1997), through to the original ASIMO (2000) and the new ASIMO (2005) [1], [2]. The P3 prototype unveiled in 1998 [3] was one of the breakthrough designs, initiating and spurring research on a number of other key platforms. The Humanoid Robot Platform (HRP) started with an adapted Honda P3 and subsequently HRP-2L/2P/2/3/4 were released [4], [5]. Similarly KAIST built KHR-1/2/3 (Hubo) [6] and Waseda continued its long and successful tradition to build many different models through to Wabian-2R [7]. The iCub humanoid represents a co-ordinated European effort in the humanoid arena aiming at producing a "child-like" humanoid platform for understanding and development of cognitive systems [8], [9], [10], but other successful humanoid/bipedal implementations within Europe include the humanoid LOLA which is an enhancement over the Johnnie robot [11]. Despite the progress made in the design of humanoids/bipeds significant barriers still remain that prevent these robots (physical structure, materials, actuation and sensing) from reaching the physical performance capabilities of the human body. These limits are particularly noticeable in adaptability during interaction and impacts, energy efficiency and mechanical robustness. Looking to the actuation system of most humanoid platforms one can see that the predominant approach is the use of non-backdrivable, stiff transmission systems, combined with high gain PID controllers. Although the non-backdrivability and the large stiffness of these robots improve their precision, the resulting large mechanical impedance imposes performance handicaps related to the ability to adapt to interaction uncertainties. On the other hand, biological systems with their soft actuation principles adapt intrinsically to interaction constraints, store and release elastic potential energy into/from muscles and tendons during normal daily activities such as walking, running, jumping, etc [12], [13], [14] and can generate motions with power peaks which could not be obtained using stiff structures and actuators. The beneficial effects of the intrinsic elasticity on specific performance aspects of the robotic systems have been also highlighted and studied in robots [15], [16], [17], [18], [19] by employing actuators with preset or variable level of compliance. Inspired by this trend, this work presents the development of COMAN, Fig. 1, a new humanoid platform with embodied passive compliance.COMAN was developed

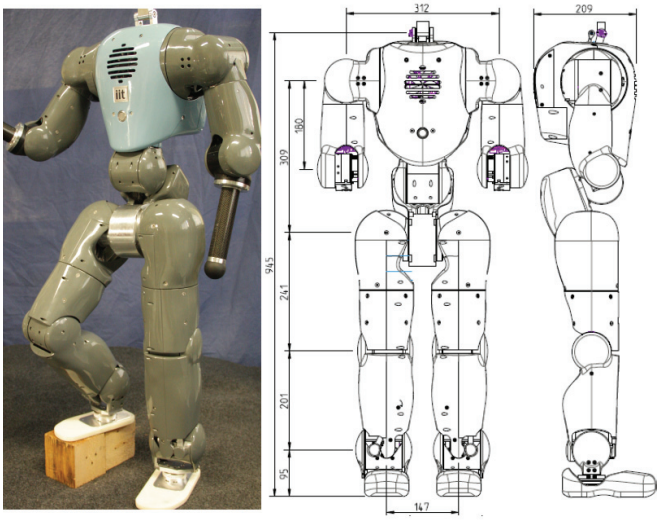

Fig. 1. Compliant humanoid COMAN, all dimensions are in (mm)

The authors are within the Department of Advanced Robotics, Istituto Italiano di Tecnologia, via Morego, 30 16163 Genova {nikos.tsagarakis, stephen.Morfey, Medrano.Cerda, Zhibin.Li, darwin.caldwell}@iit.it

978-1-4673-5643-5/13/$31.00 ©2013 IEEE

within the AMARSI European project which aims to achieve a qualitative jump toward rich motor behavior in robotic systems, rigorously following a systematic approach in which novel mechanical systems with passive compliance will be integrated with control and learning solutions. The incorporation of passively compliant actuators in a full body humanoid represents a significant achievement from the mechatronics development point of view. In this perspective a key contribution of this work is related to the selection of the joint elasticity parameters. Despite the numerous compliant robots developed in the past, the tuning of the passive elasticity of the individual joints still remains an experimental trial and error process and very little information on the criteria and methodologies used is available. For systems with large number of compliant degrees of freedom such as COMAN this trial and error process for tuning the joint elasticity is too cumbersome due to the numerous combinations of joint stiffness that can be suitable. This paper introduces a systematic method to optimally tune the joint elasticity of multi-dof compliant SEA robots based on resonance analysis and energy storage maximization criteria. The method is applied to the selection of the joint elasticity of the COMAN legs.

The paper is organized as follows: Section II gives the specifications of the compliant humanoid COMAN. Section III introduces the mechanical design of COMAN and its compliant actuation system, while Section IV presents the methodology employed to optimally tune the joint elasticity of multi-dof compliant robots based on modal analysis and energy storage maximization criteria. Section V presents experimental walking trials with COMAN and section VI addresses the conclusions.

II. General Specifications of COMAN Humanoid

The size of the COMAN humanoid robot approximates the dimensions of a 4 year old child, Fig. 1. The height of the COMAN from the foot to the center of the neck is 945mm. The width and depth at the hip is 147mm and 110mm respectively and the distance between the centers of the shoulders is 312mm. The total weight of the robot is 31.2kg with the legs and the waist module weighting $(18.5Kg)$ and the torso and the arms weighting $(12.7Kg)$. COMAN body has 25 D.O.F in total. Each leg has 6 D.O.F: 3 D.O.F at the hip, 1 D.O.F at the knee level and 2 D.O.F at the ankle. For the trunk there is a 3 D.O.F waist which each arm has currently 4 D.O.F: 3 D.O.F at the shoulder and 1 D.O.F at the elbow level. Finally a 2 D.O.F neck provides the head pitch and roll motions. In addition, to the previous generic specifications and in order to permit the experimental scenarios of the AMARSI project there was a need to incorporate compliance properties through a synergistic combination of both active and passive elasticity principles. Passive compliance based on series elastic actuation (SEA) was added to the 14 of the 25 D.O.F including all flexion/extension D.O.F of the legs, the flexion/extension of the shoulder and elbow and the shoulder abduction/adduction. Finally, the range of motion for the joints of COMAN were defined using human ergonomic data and data from other successful humanoid platforms. Table 1 shows the range of motion of the joints of COMAN.

TABLE I
RANGE OF MOTION OF JOINTS

Joint	Range of motion ()
Hip Flexion/Extension	$+45, -110$
Hip Abduction/adduction	$+60, -25$
Thigh Rotation	$+50, -50$
Knee Flexion/Extension	$+110, -10$
Ankle Flexion/Extension	$+70, -50$
Ankle Inversion/Eversion	$+35, -35$
Ankle Twist	Not Implemented
Waist Pitch	$+50, -20$
Waist Roll	$+30, -30$
Waist Yaw	$+80, -80$
Shoulder Flexion/Extension	$+95, -195$
Shoulder Abduction/adduction	$+120, -18$
Upper Arm Rotation	$+90, -90$
Elbow Flexion/Extension	$+135, 0$

III. COMAN Body Mechanics

In the mechanical construction of COMAN particular attention was paid to optimize the integration, weight and modularity of the mechanical assembly. The high density of the integration is due to the mechanical implementation of a modular series elastic actuation unit. To achieve modularity, minimize dimensions, while achieving high rotary stiffness the SEA module developed in [20] was employed to actuate the joints of COMAN. The following subsections provide details on the realization of the COMAN body subsystems.

A. Leg mechanics

COMAN leg has an anthropomorphic kinematic structure which is composed of the hip, the thigh with the knee joint, the calf with the ankle joint and the foot, Fig. 2. The hip joint is constructed as a cantilever base structure with a pitch-roll-yaw configuration. The hip pitch (flexion/extension) motion is implemented using the SEA unit (peak torque of 55Nm) while the roll and yaw motion actuators are conventional stiff modules (Kollmorgen Brushless DC motor combined with a 100:1 Harmonic reduction drive giving a peak torque of 55Nm). The hip roll motor is placed below the hip center transmitting its torque to the hip roll using a four bar mechanism, Fig. 2. The hip yaw motion is powered by an actuator enclosed inside the thigh structure. The knee joint is directly driven by a compliant actuation group (peak torque of 55Nm) at the center of the knee joint, Fig. 2. The ankle roll motion is driven by a stiff actuation unit (peak torque of 55Nm) placed at the calf. Torque to the ankle roll motion is transferred through a four bar link transmission, Fig. 2. The last D.O.F which produces ankle flexion/extension uses a SEA actuator (peak torque of 55Nm) located at the ankle center and directly coupled to the ankle pitch joint. Torque sensors developed specifically for the robot have been integrated in all joints of the leg to also permit regulation of the joint compliance through active control. In addition, custom-made 6 D.O.F force/torque sensors have been integrated below the

ankle joint to measure the interaction forces between each foot and the ground.

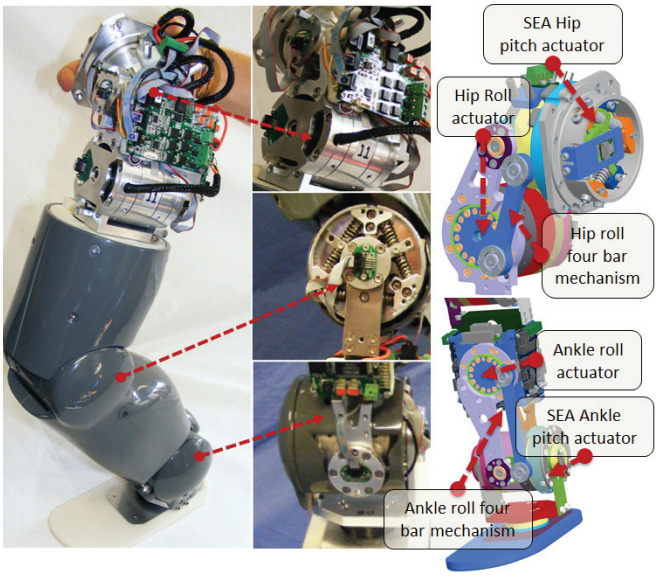

Fig. 2. Mechanical assembly of COMAN leg

B. Torso and Arm mechanics

The torso of COMAN, Fig. 3, serves as a housing for the on board processing and power units. The on-board processing unit is composed of an embedded dual core Pentium PC104 unit running at 2.5GHz. The power unit includes the battery cells and the battery management system. The battery is a custom Lithium polymer battery with a gravimetric energy density of 180Wh/Kg. The core of the torso is made in titanium alloy to give stiffness strength and low weight to this critical central structure. This structure also serves as the mounting support of the shoulder flexion D.O.F of each arm and the neck module.

The current version of the arms of COMAN has 4 D.O.F consisting of a typical pitch-roll-yaw shoulder kinematic arrangement and an elbow flexion/extension joint, Fig. 3. The shoulder flexion/extension unit is housed inside the torso and is actuated by SEA unit (peak torque of 55Nm). The shoulder abduction/adduction (roll) is also powered by a SEA unit with the same torque capacity and is placed at the center of the shoulder joint. The last shoulder D.O.F (upper arm rotation) is actuated by a stiff actuator located inside the upper arm. Finally, the elbow joint is directly driven by a SEA unit (peak torque of 55Nm), Fig. 3. No forearm hand is mounted on this variant of the COMAN although units for this have previously been shown in [21]. With regards to the actual fabrication of COMAN body most of medium/highly stressed components (motor and bearing housing and link structures) were machined from Aluminum alloy 7075 (Ergal). Joint shafts and torque sensors were fabricated from Stainless steel 17-4PH which delivers an excellent combination of good oxidation and corrosion resistance together with high strength. Body covers were made of ABS plastic using rapid prototyping fabrication.

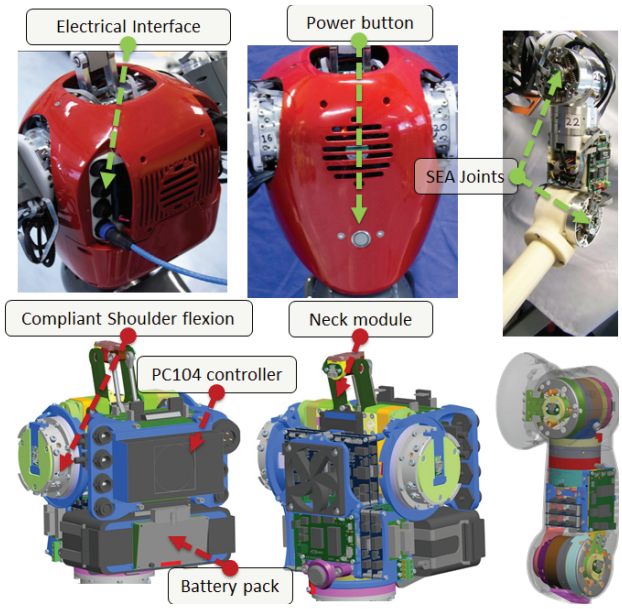

Fig. 3. Mechanical assembly of COMAN torso and arm

IV. Selection of Joint Stiffness

Despite the numerous compliant robots developed in the past, [17], [10], [22] the tuning of the stiffness of the SEA joints still remains a trial and error process and very little information on the criteria and methodologies used is available for most of these compliant robots. For systems with many compliant degrees of freedom obviously a trial and error process can be very tedious due to the numerous combinations of joint stiffness that can be selected. This section presents a systematic methodology for tuning the joint stiffness of multi-dof compliant systems powered by SEA units. This method which is experimentally applied to the design of the legs of COMAN derives optimal joint compliance levels for energy storage maximization while satisfying modal analysis criteria and constraints.

A. Compliant Body modeling

The intrinsic physical elasticity in the joints of COMAN robot results in a multi-dof nonlinear mass-spring system. To understand the behavior of the robot as far as its natural frequencies are concerned a modal study was performed on the robot body model to derive the natural frequencies for different leg configurations during the single support walking phase. The aim of this analysis was to study the effect of the joint stiffness on the modulation of the system natural frequencies. Based on this the joint stiffness can be then selected to set the resonances of the system above a specific frequency that satisfies the trajectory and control bandwidths,$\forall \omega_i : \omega_i > \alpha\omega_b$ where ω_i is i natural frequency of the robot, ω_b is the desired bandwidth and α is a scaling parameter. For the analysis presented in this work we consider the reduced model presented in Fig. 4. As depicted in Fig. 4 the full model of the series elastic driven COMAN body shown on the left was simplified to the model shown

on the right. In this simplified model all the body segments above the hips (upper body and arms) were considered as a single rigid body. During the single support phase of the

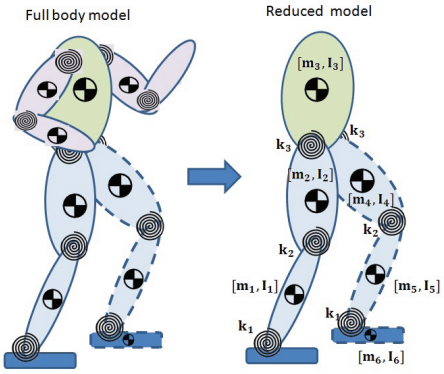

Fig. 4. COMAN whole body and reduced spring-mass model

robot in contact with ground as in Fig. 4 the dynamics of robot can be described by the following set of equations:

$$\Delta(q)\begin{bmatrix}\ddot{q}\\ \ddot{\theta}\end{bmatrix}+\Gamma(q,\ddot{q})\begin{bmatrix}\dot{q}\\ \dot{\theta}\end{bmatrix}+\begin{bmatrix}g(q)-K(\theta-q)\\ K(\theta-q)\end{bmatrix}=\begin{bmatrix}\tau_e\\ \tau_m\end{bmatrix} \quad (1)$$

where $q, \theta \in \mathcal{R}^6$ are the joint position variables at the link and motor side respectively . As only the pitch joints of the legs are equipped with series elastic actuation they have the greatest affect on the low resonance modes of the robot (the effect of the elasticity of the harmonic reduction drive, $k_h \approx 3000\frac{Nm}{rad}$ was neglected as this level of stiffness is significantly higher than the maximum achievable stiffness of 800Nm/rad permitted by the mechanical implementation of the SEA units used in COMAN). Based on this we consider in this study only the planar model along the sagittal plane. $\Delta(q) \in \mathcal{R}^{2n\times 2n}$ is the full inertia matrix.

$$\Delta(q)=\begin{bmatrix}M_L(q)+M_R(q) & \mathbf{0}\\ \mathbf{0} & B_m\end{bmatrix} \quad (2)$$

with $M_L(q))$ and $M_R(q) \in \mathcal{R}^{n\times n}$ representing the link and motor rotor inertia respectively, $B_m \in \mathcal{R}^{n\times n}$ is a diagonal motor inertia matrix and $\Gamma(q,\dot{q}) \in \mathcal{R}^{2n\times 2n}$ is the complete coriolis/centripetal and damping matrix. Note that for the case of the planar model $n = 6$, (3 D.O.F for the support leg and 3 D.O.F for the swing leg).

$$\Gamma(q,\dot{q})=\begin{bmatrix}C(q,\dot{q})+D+D_L & -D\\ -D & D+D_m\end{bmatrix} \quad (3)$$

where D, D_m and $D_L \in \mathcal{R}^{n\times n}$ are diagonal matrices corresponding to the physical damping parallel to the spring, the motor damping reflected at the output link and the link damping respectively. Finally $K \in \mathcal{R}^{n\times n}$ is the stiffness matrix with $K = diag[k_i]$ where k_i represents the stiffness of i joint and $g(q) \in \mathcal{R}^{n\times 1}$ denotes the gravity vector of the robot while τ_m and $\tau_e \in \mathcal{R}^{n\times 1}$ represent the motor and the external torque vectors respectively. By combining the link and motor side generalized coordinates q, θ into $\Theta = \begin{bmatrix} q^T & \theta^T \end{bmatrix}^T$ (1) can be formulated as

$$\Delta(q)\ddot{\Theta}+\Gamma(q,\ddot{q})\dot{\Theta}+S\Theta+G(q)=\tau \quad (4)$$

where $S=\begin{bmatrix}K & -K\\ -K & K\end{bmatrix}$ is the combined stiffness matrix, $\tau = \begin{bmatrix}\tau_e^T & \tau_m^T\end{bmatrix}^T$ is the completed torque vector and $G(q) = \begin{bmatrix} g(q)^T & 0 \end{bmatrix}^T$ is the new gravity vector. Considering now an equilibrium posture $\Theta_e = \begin{bmatrix} q_e^T & \theta_e^T \end{bmatrix}^T$ and assuming that the generalized coordinates are slightly changing around this equilibrium configuration and their time derivatives are all small then the coriolis/centripetal and damping forces can be neglected. Linearizing also the gravity vector $G(q)$ around the equilibrium configuration q_e and rearranging gives

$$\Delta(q_e)\ddot{\phi}+S_g\phi=\tau \quad (5)$$

where $\phi = \Theta - \Theta_e$ is the deviation from the equilibrium posture and $S_g=\begin{bmatrix}K & -K\\ -K & K\end{bmatrix}+\nabla G(q_e)$ is the combined stiffness matrix which includes also the gravitation effect. In the above combined matrix $\nabla G(q_e) = \begin{bmatrix}\nabla g(q_e) & \mathbf{0}\\ \mathbf{0} & \mathbf{0}\end{bmatrix}$ represents the Jacobian of the gravity vector $G(q)$ at the equilibrium position q_e . Finally consider simple proportional feedback for the motor torque, $\tau_m = k_m(\theta_e - \theta)$. Equation (5) can now be rearranged as follows

$$\Delta(q_e)\ddot{\phi}+S_{gm}\phi=\tau \quad (6)$$

where the new stiffness matrix $S_{gm} = \begin{bmatrix}K+\nabla g(q_e) & -K\\ -K & K+K_m\end{bmatrix}$ now contains also the effect of the motor active stiffness controller and $K_m \in \mathcal{R}^{n\times n}$ is the gain matrix of the motor proportional feedback with $K_m = diag[k_{m_i}]$. Equation (5) is now in the general form of the equation of motion $M\ddot{x} + Kx = f$ for a vibrating system where ϕ represents the time dependent vector that describes the motion, and $\Delta(q_e)$ and S_{gm} are mass and stiffness matrices. At its equilibrium, resonance frequencies can be obtained by determining the eigenvalues of the system dynamics. By defining $A = \Delta(q_e)^{-1}S_{gm}$ the natural frequencies around the equilibrium are given by $\omega_i^2 = \lambda_i, i = 1, 2..N$ where λ_i represents the eigenvalues of A. The resonance frequencies are therefore obtained as $f_i = \frac{1}{2\pi}\sqrt{\lambda_i}, i = 1, 2...N$.

B. Optimal Joint Stiffness Selection

In order to select the level of stiffness for the joints of the legs we formulate a constrained optimization problem with cost function which is described as follows.

$$min(\frac{1}{\sum E_i}) \quad (7)$$

where E_i denotes the potential energy stored in the i joint of the leg when the torque applied by the joint is τ_i. Equation (7) attempts to maximize the energy stored in the joints of the robot or to maximize the joint passive deflection for a given joint torque vector. The potential energy stored in the

elastic element of the joint can be expressed as a function of the applied torque τ_i and the joint stiffness, $E_i = \frac{1}{2}\frac{\tau_i^2}{k_i}$. The cost function in (7) can be then written in expanded form as

$$min(\frac{2}{\tau_i^2(\frac{1}{k_a}+\frac{1}{k_k}+\frac{1}{k_h})}) \quad (8)$$

where k_a, k_k and k_h corresponds to the stiffness of the ankle, knee and hip respectively. Note that although $K \in \mathcal{R}^{6\times6}$ due to the symmetry of the two legs there only three independent variables $K = diag\begin{bmatrix} k_a & k_k & k_h & k_h & k_k & k_a \end{bmatrix}$. In this work as a general case the torque level of each joint τ_i was set equal to the peak torque τ_{max} of the actuator. One could also consider using different peak torques for the different joints to optimize the stiffness selection for energy storage for more specific torque-peak profiles. We next introduce the inequality constraints for the optimization problem.

i) Natural Frequency inequality constraints

The natural frequency inequality constraints are selected to determine the joint stiffness required so that the robot resonances are above a specified set of frequencies ω_i. The specified frequencies ω_i a can be obtained from the walking trajectories and the control bandwidths, e.g $\forall\omega_i : \omega_i > \alpha\omega_b$ where $\alpha > 1$ is a scaling parameter. Let $f_{1r} < f_{2r} < ... < f_{nr}$ denote the n ordered robot resonant frequencies, we consider the following set of inequality constraints

$$f_{ir} : f_{ir} > \frac{\alpha_i}{2\pi}\omega_b, \alpha_i > 1, i = 1, 2, ..., n \quad (9)$$

We can thus set a maximum of n frequency constraints, and at least 1 constraint to solve the optimization problem in (8).

ii) Stiffness inequality constraints

We add two linear inequality constraints to keep the predicted joint stiffness within the physical joint limits. These constraints are of the form

$$k_{min} < k_i < k_{max} \quad (10)$$

where k_{min} and k_{max} are the minimum and maximum joint stiffness limits of the robot. The minimum stiffness level k_{min} was specified after considering the physical limits of the series elastic actuation units including their peak torque capacity τ_{max} and the limit of the maximum passive deflection θ_{smax}. Based on these two physical limits we defined k_{min} as follows

$$k_{min} = \frac{\tau_{max}}{\theta_{smax}} \quad (11)$$

Equation (11) implies that the minimum stiffness is selected to ensure that torques up to the peak torque capacity will be transmitted through the series elasticity, preventing it from reaching the limit of the passive deflection of the elastic element for the full range of the actuator torque. For the SEA units used in COMAN $k_{min} = \frac{55Nm}{0.2rad} = 275\frac{Nm}{rad}$. Regarding the maximum stiffness, this was set four times lower $k_{max} = 800\frac{Nm}{rad}$ than the stiffness of the harmonic reduction drive $k_h \approx 3000\frac{Nm}{rad}$ ensuring the validity of neglecting the effect of harmonic drive stiffness in the resonance analysis study. Using the cost function in (8) and the inequalities constraints reported before we performed an optimization to find the stiffness of the legs joints that satisfied the constraints while minimizing the cost function in (8). The optimization was performed with MATLAB's Optimization Toolbox and the FMINCON function using multi-start methods with a large number of initial conditions scattered around the joint stiffness range. Figure 5 presents the resulting optimal stiffness selection for twenty different posture configuration points of the single support phase. It can been seen that the stiffness changes as a function of the configuration with this effect being most obvious for the hip joint. In this optimization, the two frequency constraints chosen were for the lowest resonant frequency f_1 to be larger than 1.0Hz ($f_1 > 1.0Hz$) and for the second lowest resonant frequency f_2 to be above $3.0Hz$ ($f_2 > 3.0Hz$). The level of stiffness finally selected for the joint of COMAN is given from the maximum value of the corresponding curve shown in Fig. 5. This results in the following leg stiffness set $(k_a, k_k, k_h) = (597, 417, 396)Nm/rad$. Fig. 6 presents

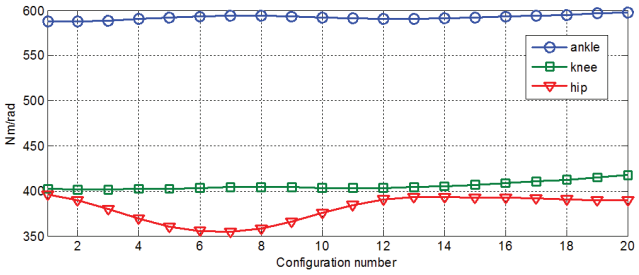

Fig. 5. Optimal leg joint stiffness as a function of the single support posture configuration: First and second natural frequencies inequalities constraints: ($f_1 > 1.0Hz$ and $f_2 > 3.0Hz$)

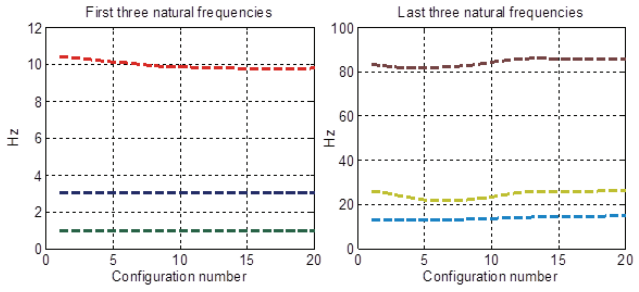

Fig. 6. Natural frequencies as a function of the configuration and the optimal stiffness of the configuration, first two frequencies are fixed to $f_1 = 1.0Hz$ and $f_2 = 3.0Hz$

the resultant natural frequencies given a body configuration its corresponding optimal stiffness matrix. It can be observed that when selecting the optimal joint stiffness according to Fig. 5 the first and the second natural frequencies remain constant to $1.0Hz$ and $3.0Hz$ respectively as defined by the natural frequencies inequalities constraints.

V. COMAN Experimental Trials

To validate the functionality of COMAN, the walking pattern generation method developed in [23] was implemented.

The snapshots of successful walking is shown in Fig. 7. Fig. 8 shows the ground reaction force applied on each foot. Despite the force spikes at the very beginning of the foot landing, the overall ground reaction force keeps around the body weight of the robot. This is achieved naturally and costless by merely the hardware itself without additional control enforcement which is difficult to be realized by the stiff actuated humanoids if no particular foot mechanism or active control is applied.

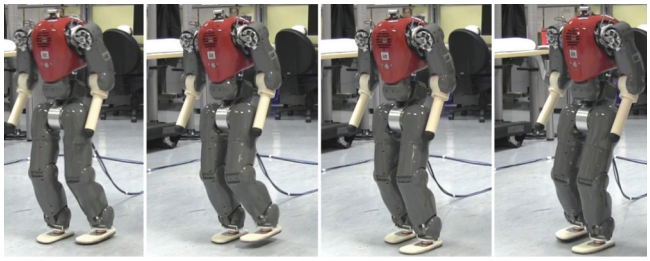

Fig. 7. Snapshots of COMAN walking

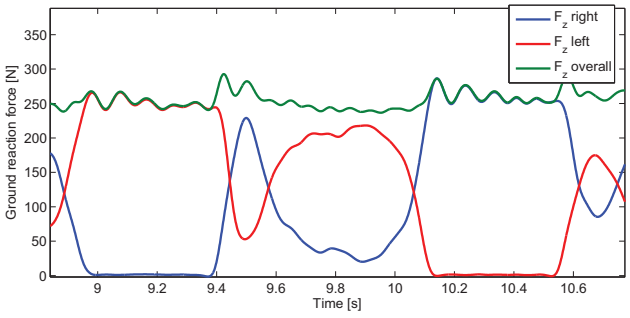

Fig. 8. The vertical ground reaction force applied on COMAN's feet

VI. Conclusions

This work introduced the compliant humanoid COMAN. Fourteen of the 25 D.O.F of the robot are powered by series elastic actuators. The realization of a whole body passively compliant humanoid platform represents by itself a significant development from the mechatronics perspective. The overall design of the COMAN was presented including details on the mechanisms and construction of the different body modules and sections. The selection of the level of elasticity/stiffness in the different joints of such a multi-dof robot is not a trivial task and despite the numerous compliant robots developed in the past the tuning of the stiffness of the individual joints still remains an experimental trial and error process with very little literature on the criteria and methodologies used. We complemented the mechatronics development with a systematic methodology on the joint stiffness tuning based on modal analysis and energy storage maximization criteria. The working functionality of COMAN was finally demonstrated during bipedal locomotion trials.

Acknowledgment

This work is supported by the European Commission projects AMARSI and SAPHARI.

References

[1] K. Hirai, Y. Hirose, Y. Haikawa, and T. Takenaka. The development of honda humanoid robot. In *IEEE ICRA*, pages 1321 – 1326, 1998.

[2] M. Hirose, Y. Haikawa, T. Takenaka, and K. Hirai. Development of humanoid robot asimo. In *IEEE IROS Workshop*, 2001.

[3] M. Hirose and K. Ogawa. Honda humanoid robots development. *Philosophical Transactions of the Royal Society A: Mathematical, Physical and Engineering Sciences*, pages 11 – 19, 2007.

[4] K. Akachi, K. Kaneko, S. Ota, G. Miyamori, M. Mirata, S. Kajita, and F. Kanehiro. Development of humanoid robot hrp-3p. In *IEEE-RAS Int. Conf. on Humanoid Robots*, pages 50 – 55, 2005.

[5] K. Kaneko, K. Harada, F. Kanehiro, G. Miyamori, and K. Akachi. Humanoid robot hrp-3. In *IEEE IROS*, pages 2471 – 2478, 2008.

[6] I.W. Park, J.Lee Kim, and J.H. Oh. Mechanical design of the humanoid robot platform hubo. *Journal of Advanced Robotics*, 21(11):1305 – 1322, 2007.

[7] Y. Ogura, H. Aikawa, A. Shimomura, A. Morishima, and Takanishi A. Lim, H. Development of a new humanoid robot wabian-2. In *IEEE ICRA*, pages 76 – 81, 2006.

[8] G. Metta, G. Sandini, D. Vernon, D.G. Caldwell, N.G. Tsagarakis, R. Beira, J.S. Victor, A.J. Ijspeert, L. Righetti, G. Cappiello, G. Stellini, and F. Becchi. The robotcub project-an open framework for research in embodied cognition. In *IEEERAS International Conference on Humanoid Robots, Workshop*, 2005.

[9] N.G. Tsagarakis, F. Becchi, L. Righetti, A. Ijspeert, and D.G. Caldwell. Lower body realization of the baby humanoid icub. In *IEEE IROS*, pages 3616–3622, 2007.

[10] N.G. Tsagarakis, Li. Zhibin, J.A. Saglia, and Caldwell D.G. The design of the lower body of the compliant humanoid robot ccub. In *IEEE ICRA*, pages 2035–2040, 2011.

[11] S. Lohmeier, T. Buschmann, H. Ulbrich, and F. Pfeiffer. Modular joint design for performance enhanced humanoid robot lola. In *IEEE ICRA*, pages 88 – 93, 2006.

[12] M. Ishikawa, P.V. Komi, G.V. Lepola, and G.P. Bruggemann. Muscle-tendon interaction and elastic energy usage in human walking. *J Appl Physiol*, 99(2):603–608, 2005.

[13] M. Laffranchi, N.G. Tsagarakis, and D.G. Caldwell. Antagonistic and series elastic actuators: a comparative analysis on the energy consumption. In *IEEE IROS*, pages 5678 – 5684, 2009.

[14] T.J. Roberts, R.L. Marsh, P.G. Weyand, and C.R. Taylor. Muscle-tendon interaction and elastic energy usage in human walking. *Science*, 275(5303):1113–1115, 1997.

[15] G. Pratt and M. Williamson. Series elastic actuators. In *IEEE IROS*, pages 399–406, 1995.

[16] M. Garabini, A. Passaglia, F. A. W. Belo, P. Salaris, and A. Bicchi. Optimality principles in variable stiffness control: the vsa hammer. In *IEEE IROS*, pages 3770 – 3775, 2011.

[17] J. Hurst. The electric cable differential leg: A novel design approach for walking and running. *Journal of Humanoid Robots*, 8(2):301 – 321, 2011.

[18] Zhibin Li, N.G. Tsagarakis, and D.G. Caldwell. A passivity based admittance control for stabilizing the compliant humanoid COMAN. In *IEEE-RAS International Conference on Humanoid Robots*, pages 44–49, Osaka, Japan, Nov. 29th - Dec. 1st 2012.

[19] L. Chen, M. Garabini, M. Laffranchi, N. Kashiri, N.G. Tsagarakis, A. Bicchi, and D.G. Caldwell. Optimal control for maximizing velocity of the compact compliant actuator. In *IEEE ICRA*, 2013.

[20] N.G. Tsagarakis, M. Laffranchi, B. Vanderborght, and D.G Caldwell. A compact soft actuator for small scale robotic systems. In *IEEE ICRA*, pages 4356 – 4362, 2009.

[21] S. Davis, N.G. Tsagarakis, and D.G. Caldwell. The initial design and manufacturing process of a low cost hand for the robot icub. In *IEEE Humanoids*, pages 40–45, 2008.

[22] J. Pratt, T. Koolen, T. De Boer, J. Rebula, S. Cotton, J. Carff, M. Johnson, and P. Neuhaus. Capturability-based analysis and control of legged locomotion, part 2: Application to m2v2, a lower-body humanoid. *International Journal of Robotics Research*, 31:1117–1133, 2012.

[23] Zhibin Li, N.G. Tsagarakis, and Darwin G. Caldwell. Walking trajectory generation for humanoid robots with compliant joints: Experimentation with coman humanoid. In *IEEE ICRA*, pages 836 – 841, Minnesota, USA, May 2012.